Petroleum Science 22 (2025) 1051–1061

Contents lists available at ScienceDirect

Petroleum Science

journal homepage: www.keaipublishing.com/en/journals/petroleum-science

Original Paper

A robust seismic wavefield modeling method based on minimizing spatial simulation error using L_2-norm cost function

Wei-Ting Peng [a, b], Jian-Ping Huang [a, b, *]

[a] Geosciences Department, China University of Petroleum (East China), Qingdao, 266580, Shandong, China
[b] Pilot National Laboratory for Marine Science and Technology (Qingdao), Qingdao, 266000, Shandong, China

ARTICLE INFO

Article history:
Received 29 March 2024
Received in revised form
8 August 2024
Accepted 2 December 2024
Available online 4 December 2024

Edited by Meng-Jiao Zhou and Min Li

Keywords:
Finite-difference scheme
FD coefficients
Spatial simulation error
Spatial dispersion relation
Seismic wavefield

ABSTRACT

To reduce the spatial simulation error generated by the finite difference method, previous researchers compute the optimal finite-difference weights always by minimizing the error of spatial dispersion relation. However, we prove that the spatial simulation error of the finite difference method is associated with the dot product of the spatial dispersion relation of the finite-difference weights and the spectrum of the seismic wavefield. Based on the dot product relation, we construct a L_2 norm cost function to minimize spatial simulation error. For solving this optimization problem, the seismic wavefield information in wavenumber region is necessary. Nevertheless, the seismic wavefield is generally obtained by costly forward modeling techniques. To reduce the computational cost, we substitute the spectrum of the seismic wavelet for the spectrum of the seismic wavefield, as the seismic wavelet plays a key role in determining the seismic wavefield. In solving the optimization problem, we design an exhaustive search method to obtain the solution of the L_2 norm optimization problem. After solving the optimization problem, we are able to achieve the finite-difference weights that minimize spatial simulation error. In theoretical error analyses, the finite-difference weights from the proposed method can output more accurate simulation results compared to those from previous optimization algorithms. Furthermore, we validate our method through numerical tests with synthetic models, which encompass homogenous/inhomogeneous media as well as isotropic and anisotropic media.

1. Introduction

The finite-difference (FD) method has been a widely employed technique for numerical simulations of seismic wave propagation. The popularity of the FD method is primarily due to its low computational cost and straightforward implementation (Alterman et al., 1968; Kelly et al., 1976). However, the inherent errors of this simulation technique are inevitable due to the omission of the higher-order infinitesimal term and truncation error term during the derivation of the FD scheme (Alford et al., 1974; Dablain, 1986). These errors can be divided into spatial simulation error and temporal simulation error. To minimize the spatial simulation error, choosing FD weights with broad bandwidth can be considered, for which the FD scheme functions exactly (Holberg, 1987; Kindelan et al., 1990; Zhou and Greenhalgh, 1992).

Many efforts have been made to compute the FD weights. One of the common ways is using optimization methods, with different norms, including the L_∞ norm (Holberg, 1987; Kindelan et al., 1990; Zhang and Yao, 2013a, 2013b; Yang et al., 2017a, 2017b; He et al., 2019; Koene and Robertsson, 2020; Liu, 2020a), the L_2 norm (Wang and Wu, 2002; Etgen, 2007; Liu, 2013, 2014; Wang et al., 2014; Ren and Liu, 2015; Yong et al., 2017) and the L_1 norm (Miao and Zhang, 2020). Another strategy for computing FD weights is to adopt a specific window function to truncate the pseudospectra of the wavefield to compute the FD weights (Zhou and Greenhalgh, 1992; Igel et al., 1995; Shao et al., 2003; Xiao et al., 2006; Chu et al., 2009; Chu and Stoffa, 2012).

For numerical modeling, the ideal FD scheme requires FD weights that generate no error across all frequencies. In simpler terms, FD weights should preserve the dispersion relation without dispersion error across the entire wavenumber spectrum. Although geophysicists have not yet discovered such perfect FD weights, they have proposed two criteria as a means to approach it. One is that FD weights have as a wide bandwidth as possible within a given

* Corresponding author.
E-mail address: jphuang@upc.edu.cn (J.-P. Huang).

https://doi.org/10.1016/j.petsci.2024.12.003

dispersion error limitation, and the other is that FD weights have as small a low-wavenumber dispersion error amplitude as possible within a given bandwidth (Koene and Robertsson, 2020).

Based on the first criterion, the Remez exchange algorithm (REA) (He et al., 2019; Koene and Robertsson, 2020; Remez, 1934; McClellan et al., 1973) produces the FD weights with the broadest bandwidth among all these methods. This characteristic can be attributed to its equiripple property. When evaluating existing methods according to the second criterion, the Alternating direction multiplier method (ADMM) with L_1 norm optimization problem (Miao and Zhang, 2020) is an optimal choice. That is because the ADMM's solution has the least low-wavenumber dispersion error.

In the practical test, researchers found some interesting observations. In numerical modeling, when the energy of the seismic wavefield concentrates in the high wavenumber region, FD weights from REA output simulation result with less spatial simulation error than other optimization algorithms (He et al., 2019). Conversely, FD weights from ADMM can provide more accurate wavefield records than REA when the energy of the seismic wavefield tends towards the low-wavenumber region (Miao and Zhang, 2020). These phenomena indicate that when the energy of the seismic wavefield changes, it is difficult for an optimization method to consistently output modeling results with the least spatial simulation error.

In this paper, we proved that the spatial simulation error is a dot product of the spatial dispersion relation with the spectrum of the seismic wavefield. The previous methods considered minimizing the error of spatial dispersion relation, not the spatial simulation error, thus, they can't consistently simulate accurate seismic wavefield. We then carried out a test to verify this conclusion using REA and the Taylor expansion method in the space domain (TES). For minimizing spatial the simulation error, we formulated an L_2 norm optimization problem based on the dot product of the spatial dispersion relation with the spectrum of the seismic wavefield, and used an exhaustive search method to solve this problem. We used a sampling approximation method (SAM) to calculate the FD weights in this paper. This method can provide more selections in FD weights than other optimization algorithms. The sampling points are special M wavenumbers proposed by Peng et al. (2023). By solving this L_2 norm optimization problem, we can obtain the optimal FD weights. To assess the effectiveness of the new FD weights, we compared them with the weights obtained via TES and REA across both homogeneous and inhomogeneous media seismograms.

2. Theory

2.1. Spatial simulation error

In a square grid system, a 2*M*th-order discretization of the second spatial derivative can be expressed as (Levander, 1988; Fornberg, 1995; Liu, 2020b)

$$\frac{\partial^2 u(x)}{\partial x^2} \approx \frac{1}{h^2}\left\{c_0 u(x) + \sum_{m=1}^{M} c_m [u(x+mh) + u(x-mh)]\right\} \tag{1}$$

where the $u(x)$ is scalar pressure wavefield, h is grid point spacing, c_0 and c_m are FD weights. According to the plane wave theory, the wavefiled $u(x+mh)$ can be expressed as

$$u(x+mh) = u_0 e^{ik(x+mh)} \tag{2}$$

where e represents the natural constant, u_0 is a constant value for wavefield amplitude. Substituting Eq. (2) into Eq. (1), we can transform the spatial domain FD operator (Eq. (1)) into the wavenumber domain,

$$-k^2 h^2 U(k) \approx U(k)\left[c_0 + 2\sum_{m=1}^{M} c_m \cos(mkh)\right] \tag{3}$$

where the $U(k)$ represents the spectrum of the seismic wavefield $u(x)$. When $k = 0$, the $c_0 = -2\sum_{m=1}^{M} c_m$. According to this, Eq. (3) can be rewritten as

$$-(kh)^2 U(k) \approx U(k) 2\sum_{m=1}^{M} c_m[\cos(mkh) - 1] \tag{4}$$

Eq. (4) can be abbreviated to

$$B_a U(k) \approx U(k) B_n \tag{5}$$

where the B_a is the real or accurate wavenumber, and B_a represents $-(kh)^2$; the B_n is the numerical wavenumber, and B_n represents $\sum_{m=1}^{M} c_m[\cos(mkh) - 1]$. Thus, the spatial simulation error generated from spatial derivative can be derived by

$$E = \int_0^{k_{max}} \left(\frac{B_n}{B_a} - 1\right) U(k) \mathrm{d}k = \int_0^{k_{max}} B(c_m, k) U(k) \mathrm{d}k \tag{6}$$

where the E denotes as the spatial simulation error between the precision wavefield and the simulated wavefield, neglecting temporal error, the $B(c_m, k)$ represents the relative spatial dispersion relation, k_{max} is the maximum wavenumber. kh ranges from 0 to π because the maximal kh is on par with π according to the Nyquist theorem. Thus the k_{max} is equal to $\frac{\pi}{h}$. Eq. (6) can be rewritten as

$$E = \int_0^{\frac{\pi}{h}} B(c_m, k) U(k) \mathrm{d}k \tag{7}$$

Theoretically, we should minimize E to optimize the FD weights to reduce simulation error. However, in previous cases, researchers focused on minimizing $B(c_m, k)$, not $E(k)$, to obtain optimized FD weights, overlooking the influence of the wavefield $U(k)$. Consequently, in some simulation experiments, optimized FD weights lead to even larger spatial simulation errors.

To verify the previous conclusion regarding spatial simulation error, we employed the Remez exchange method and the Taylor expansion method for testing. The Remez exchange method is a widely used algorithm to compute FD weights proposed by He et al. (2019) for reducing spatial simulation error. The Taylor expansion method is a convolution method used to compute FD weights. The relative spatial dispersion of REA and TES is computed by $\left(\frac{B_n}{B_a} - 1\right)$, as shown in Fig. 1. When the dominant frequency of the Ricker wavelet is 40 Hz, h is 5 m, τ is 0.1 ms, velocity is 2000 m/s, the spectrum of the 1D seismic wavefield (U) is shown in Fig. 2. According to Eq. (7), the spatial simulation error (E) is shown in Fig. 3. It was observed that the spatial simulation error of REA was larger than that of TES. The optimized FD weights didn't reduce spatial simulation error because they were obtained by minimizing $B(c_m, k)$ not $E(k)$.

2.2. Minimizing spatial simulation error E

In previous section, we have proven that minimizing the error of the dispersion relation $B(c_m, k)$ is not the optimal way to reduce the spatial simulation error. Thus, we should minimize the spatial simulation error directly. Minimizing the spatial simulation error is

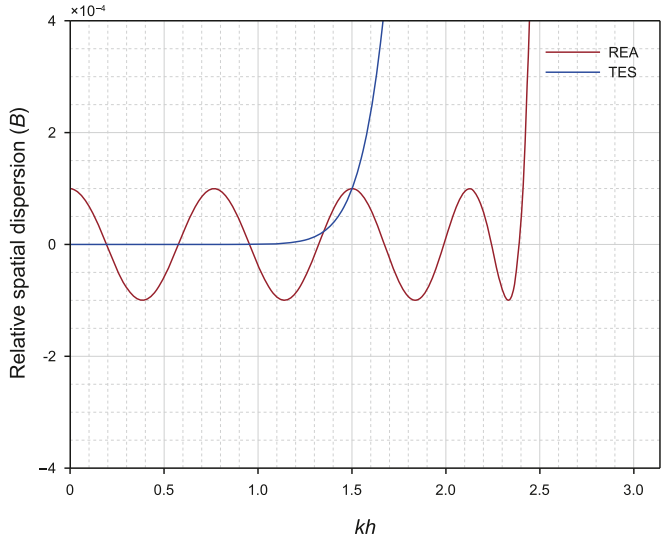

Fig. 1. A comparison of the relative spatial dispersion curves of REA and TES FD weights.

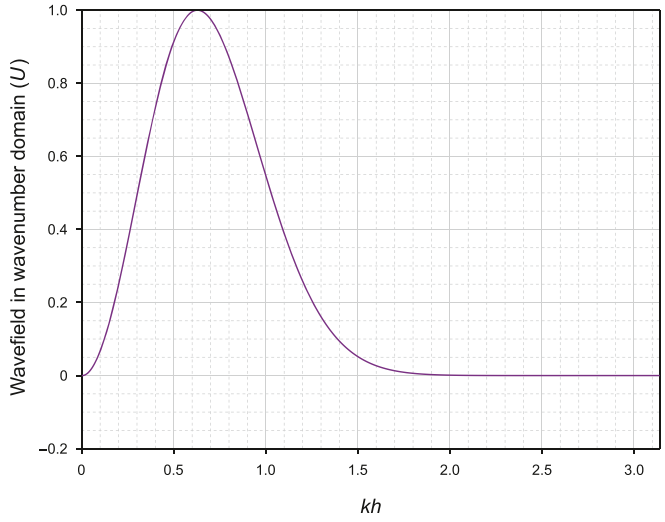

Fig. 2. The spectrum of 1D seismic wavefield in wavenumber domain.

a classical optimal problem involving two variables, $B(c_m, k)$ and $U(k)$. $U(k)$ is the seismic wavefield and cannot be equal to 0. In an ideal situation, when $B(c_m, k)$ is equal to 0, the simulation error is also equal to 0. However, in practical computations, achieving $B(c_m, k)$ equal to 0 was difficult. Based on Eq. (7), we constructed an optimization problem for the global minimum,

$$L = \left\| \int_0^{\frac{\pi}{h}} B(c_m, k) U(k) \mathrm{d}k \right\|_2^2 \tag{8}$$

$U(k)$ is the spectrum of the seismic wavefield. Iteratively updating the $U(k)$ implies performing multiple forward modeling. Even with the fastest forward simulation algorithms, the computational costs remain unacceptable. In practical numerical modeling, the spectrum of the seismic wavelet is mainly determined by the spectrum of the seismic wavefield. To solve this optimization problem, we replaced the spectrum of the seismic wavefield $U(k)$ with the spectrum of seismic wavelet $U_{\mathrm{w}}(k)$. Therefore, when simulation parameters are determined, the $U_{\mathrm{w}}(k)$ becomes a known vector not

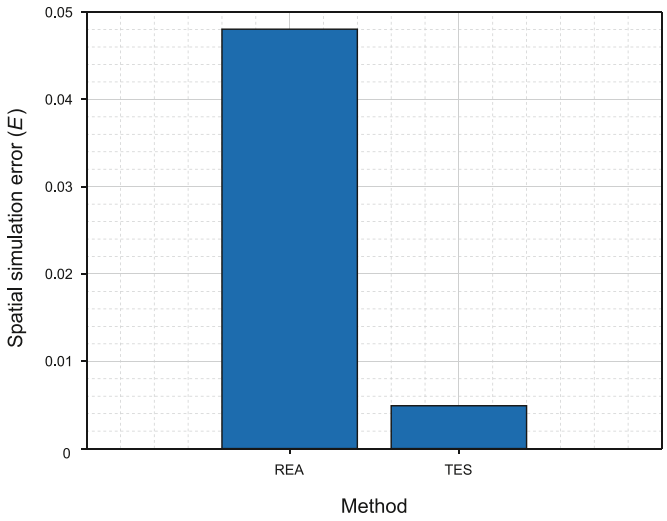

Fig. 3. Spatial simulation error of REA and TES. The spatial simulation error is computed based on Eq. (7), which is the dot product of the relative spatial dispersion curves ($B(c_m, k)$) with the spectrum of the 1D seismic wavefield ($U(k)$).

a variable. Thus the new optimization problem can be rewritten as

$$L = \left\| \int_0^{\frac{\pi}{h}} B(c_m, k) U_{\mathrm{w}}(k) \mathrm{d}k \right\|_2^2 \tag{9}$$

We used the exhaustion method to solving the optimization problem. The specific algorithm workflow is shown in Algorithm 1.

Algorithm 1. The workflow of minimizing E

Input parameter: $M, f_{\mathrm{m}}, v_{\mathrm{ave}}, h, \tau, t,$
Compute $w(t)$, $w(t)$ = ricker_wavelet$(f_{\mathrm{m}}, \tau, t)$
Compute $W(f)$, $W(f)$ = fft$[w(t)]$
Compute $U_{\mathrm{w}}(k)$, $U_{\mathrm{w}}(k) = \frac{2\pi h}{v_{\mathrm{ave}}} W(f)$ iteration
1. update the c_m, c_m = SAM(M)
2. update the E, $E = B(\boldsymbol{c})U_{\mathrm{w}}$
Output: c_m

In the algorithm, ricker_wavelet represents a computer program that generates a time-series seismic wavelet based on parameters. τ is the time step, t is the propagation time, and f_{m} represents the dominant frequency of the wavelet. The "fft" in Algorithm 1 implies a Fourier transform program. We transformed the spectrum of seismic wavelet from the frequency domain to the wavenumber domain using $\frac{2\pi h}{v_{\mathrm{ave}}} W(f)$, v_{ave} represents the estimated average velocity based on the velocity model and propagation time.

We used the sampling approximating method (SAM) to compute $B(c_m, k)$, because SAM can provide more options of FD weights compared to traditional optimization algorithms like Least-squares method (LSM) (Liu (2013), REA and ADMM in the selection of $B(c_m, k)$.

2.3. The sampling approximating method

For the sampling approximating method, the most important element is the sampling. We adopted interesting special wavenumbers proposed by Peng et al. (2023) as the sampling. These wavenumbers can be expressed as

$$\boldsymbol{b} = \boldsymbol{b}^i - p \tag{10}$$

where $\boldsymbol{b}, b_j = k_j h (j = 1, 2, 3, \ldots, M)$ are denoted as the special M wavenumbers in Peng et al. (2023), b_j are mutually distinct, $\boldsymbol{b}^i$ are initial wavenumbers obtained by optimization algorithms, like REA, LSM and ADMM (Peng et al., 2023), and p is a positive value. By substituting the special M wavenumbers into the spatial dispersion relation $B(c_m, k)$, we can express the resulting linear system of equations as follows:

$$0 = \frac{2\sum_{m=1}^{M} c_m \left[\cos(mb_j) - 1\right]}{-b_j^2} - 1 \quad (j = 1, 2, 3 \ldots, M) \tag{11}$$

The expansion of Eq. (11) can be expressed as Yang et al. (2017a, 2017b).

$$\begin{vmatrix} \frac{\cos(1b_1)-1}{b_1^2} & \frac{\cos(2b_1)-1}{b_1^2} & \cdots & \frac{\cos(Mb_1)-1}{b_1^2} \\ \frac{\cos(1b_2)-1}{b_2^2} & \frac{\cos(2b_2)-1}{b_2^2} & \cdots & \frac{\cos(Mb_2)-1}{b_2^2} \\ \vdots & \vdots & \cdots & \vdots \\ \frac{\cos(1b_M)-1}{b_M^2} & \frac{\cos(2b_M)-1}{b_M^2} & \cdots & \frac{\cos(Mb_M)-1}{b_M^2} \end{vmatrix} \times \begin{vmatrix} c_1 \\ c_2 \\ \vdots \\ c_M \end{vmatrix} = \begin{vmatrix} -1 \\ -1 \\ \vdots \\ -1 \end{vmatrix} \tag{12}$$

Eq. (12) can be rewritten as

$$\boldsymbol{A}(\boldsymbol{b})\boldsymbol{c} = \mathbf{d} \tag{13}$$

where $\boldsymbol{A} \in \mathbb{R}^{\mathbf{M}\times\mathbf{M}}$. There is an interesting fact regarding the rank of $\boldsymbol{A}$. If the rank of $\boldsymbol{A}$ and the rank of the augmented matrix $(\boldsymbol{A}\ \mathbf{d})$ are both equal to M, a linear system of equations (Eq. (13)) has only one solution according to linear algebra theory. Thus, a set of special M wavenumbers can only compute one set of FD weights using the SAM. The SAM solution is of an analytical nature. Unlike the solutions of traditional optimization algorithms (REA, LSM, ADMM), they are influenced by the initial parameters or the number of iterations. The FD weights of SAM can be obtained using the formulation,

$$\boldsymbol{c} = \boldsymbol{A}^{-1}(\boldsymbol{b})\mathbf{d} \tag{14}$$

If we use traditional optimization algorithms to calculate FD weights, we can only obtain one set of FD weights under a fixed error tolerance, thus having only one $B(c_m, k)$ to choose from. However, in Eq. (14), because sampling point $\boldsymbol{b}$ is obtained by $\boldsymbol{b} = \boldsymbol{b}^i - p$, we can obtain different sets of sampling points by adjusting $\boldsymbol{b}^i$ and p. This adjustment operation allows us to compute multiple sets of FD weights under a fixed error tolerance using the SAM. Having multiple sets of FD weights under fixed error tolerance means that SAM can obtain multiple $B(c_m, k)$ within the same condition. The adjusting operation of $\boldsymbol{b}^i$ and p is as follows: when $\boldsymbol{b}^i$ increases, p increases, and when $\boldsymbol{b}^i$ decreases, p decreases. The stability of the SAM is discussed in the Appendix.

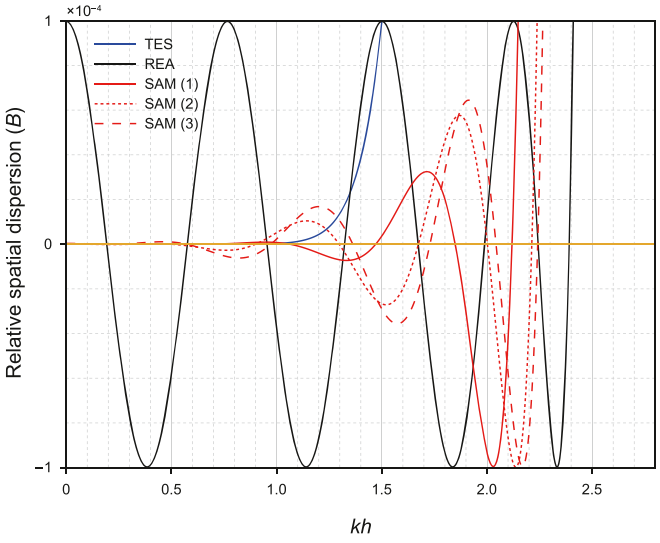

Fig. 4. A comparison of the relative spatial dispersion cuves of REA, SAM and TES FD weights.

3. Theoretical error analyses

In this section, we presented two analyses. The first is the dispersion relation analysis with the objective of substantiating that the SAM is capable of computing multiple sets of FD weights in the fixed error tolerance. The second is the performance analysis of generating the spatial simulation error aimed at illustrating that the new method yields the least possible spatial simulation error. we compared three methods, REA (He et al., 2019), TES, and the proposed method.

Three sets of FD weights were computed for the same error tolerance, as shown in Fig. 4. In Fig. 4, each curve represents a set of FD weights. It can be observed that the FD weights from REA provide the broadest bandwidth under the same error tolerance, covering approximately 10.87% more wavenumber region than the SAM (1), as shown in Fig. 4. It is notable that REA and TES can only

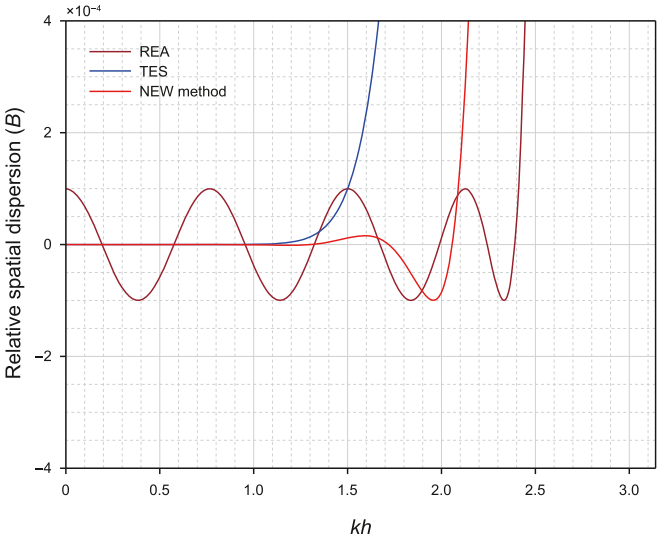

Fig. 5. A comparison of the relative spatial dispersion cuves of REA, new method and TES FD weights.

Table 1
The FD weights from different methods in Figs. 4 and 5.

REA	TES	SAM(1)	SAM(2)	SAM(2)	New method
1.912412497025990	1.777777777784810	1.864517970221300	1.880668867640410	1.885668321928440	1.854430786977060
−0.417184277546726	−0.311111111114948	−0.376311324915703	−0.389719458881255	−0.393949481583229	−0.368142207009117
0.146712622154826	0.075420875422329	0.115572189232860	0.125288699838556	0.128459492669186	0.109912375118199
−0.058492929938945	−0.017676767677177	−0.037600700228116	−0.043613618140840	−0.045682172944097	−0.034334479820169
0.023249417163344	0.003480963481052	0.011207631860865	0.014257228305223	0.015390711103540	0.009705908143951
−0.008430453541392	−0.000518000518014	−0.002730864268395	−0.003908072932626	−0.004393300147087	−0.002218964665582
0.002456117364094	0.000050742907887	0.000468683302011	0.000770819789720	0.000911505469580	0.000354711747233
−0.000412354204683	−0.000002428127428	−0.000041505840026	−0.000079402533614	−0.000099439779392	−0.000029179832109

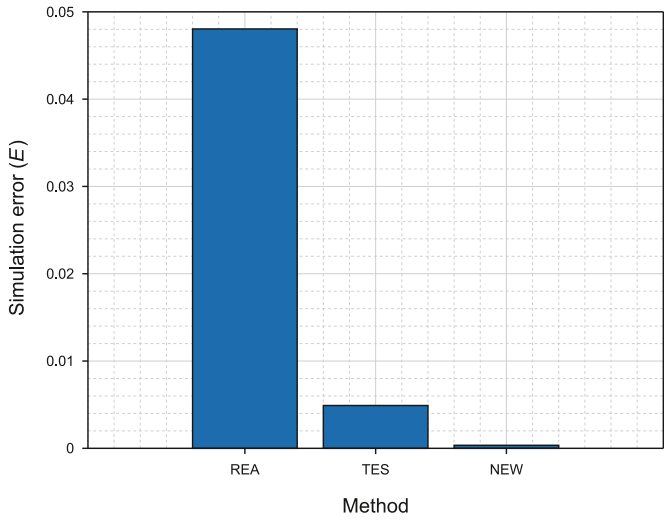

Fig. 6. Spatial simulation error of REA, new method and TES. The spatial simulation error is computed based on Eq. (7), which is dot product of the relative spatial dispersion curves ($B(c_m, k)$) with spectrum of 1D seismic wavefield ($U(k)$).

output one dispersion relation curve; however, SAM can output numerous dispersion relation curves (we only show three curves) as shown in Fig. 4. This illustrates that SAM can provide more choices of FD weights for minimizing E than conventional optimization methods. The FD weights used to plot the curves are presented in Table 1.

Next, we conducted a spatial simulation error evaluation test on the new method using experimental parameters identical to those used in previous spatial simulation error evaluations. According to these experimental parameters, the FD weights from the new method were obtained using Algorithm 1. The results for spatial dispersion relation (B) and spatial simulation error (E) are shown in Figs. 5 and 6. From Fig. 6, we observe that the new method effectively reduces the spatial simulation error E compared with the REA and TES methods. The FD weights involved in plotting the curves are listed in Table 1.

4. Numerical simulations

4.1. Homogeneous model simulation

We examined the effectiveness and validity of the new method using a homogeneous model. The Ricker wavelet was used as the source-time function in our numerical experiments. The dominant frequency of the Ricker wavelet is 40 Hz. The homogeneous media had a velocity of 2000 m/s for 1000×1000 grids with 5 m size, a time step of 0.0001 s, and a model for 1 s. A small time step was selected to avoid temporal simulation error. The source was injected at (2500 m, 2500 m). In homogeneous modeling, we used 16-th order FD weights to simulate the seismic snap. The FD weights were computed by three methods, TES, REA and the new method. The optimized FD weights were computed based on the same error tolerance. The FD weights used in the modeling test are listed in Table 2, and are displayed to 15 decimal places to accurately demonstrate their numerical results.

Fig. 7 shows that the snap residual is the difference between the analytical and FD solutions. The parameters of this homogeneous model simulation are identical to those of the spatial simulation error evaluation test. Furthermore, we observed that the snap residual of the new method was the smallest, followed by the TES method, and the REA method had the largest snap residual. This phenomenon is consistent with the observations from the spatial simulation error evaluation test, demonstrating that minimizing E is the most effective way to reduce spatial simulation error.

To test whether the new method is robust to parameter variations, we modified the spatial sampling interval to 6 m and set the injection point of the wavelet to (3000 m, 3000 m), while keeping other parameters constant. The residual of the snapshots was shown in Fig. 8. Among the three methods, the snap residual of the new method was the smallest. These two sets of model simulations demonstrate that the new method can consistently output optimal FD solutions in a homogeneous model, thereby indicating its robustness.

4.2. Inhomogeneous model simulation

To validate the performance of the new method in a complex

Table 2
The FD weights from different methods in homogeneous model simulation.

REA	TES	New method (dx = 5 m)	New method (dx = 6 m)
1.912412497025990	1.777777777784810	1.854430786977060	1.854557128963670
−0.417184277546726	−0.311111111114948	−0.368142207009117	−0.368242917960523
0.146712622154826	0.075420875422329	0.109912375118199	0.109980209087154
−0.058492929938945	−0.017676767677177	−0.034334479820169	−0.034372016707160
0.023249417163344	0.003480963481052	0.009705908143951	0.009722233478347
−0.008430453541392	−0.000518000518014	−0.002218964665582	−0.002224168345644
0.002456117364094	0.000050742907887	0.000354711747233	0.000355786209111
−0.000412354204683	−0.000002428127428	−0.000029179832109	−0.000029287070676

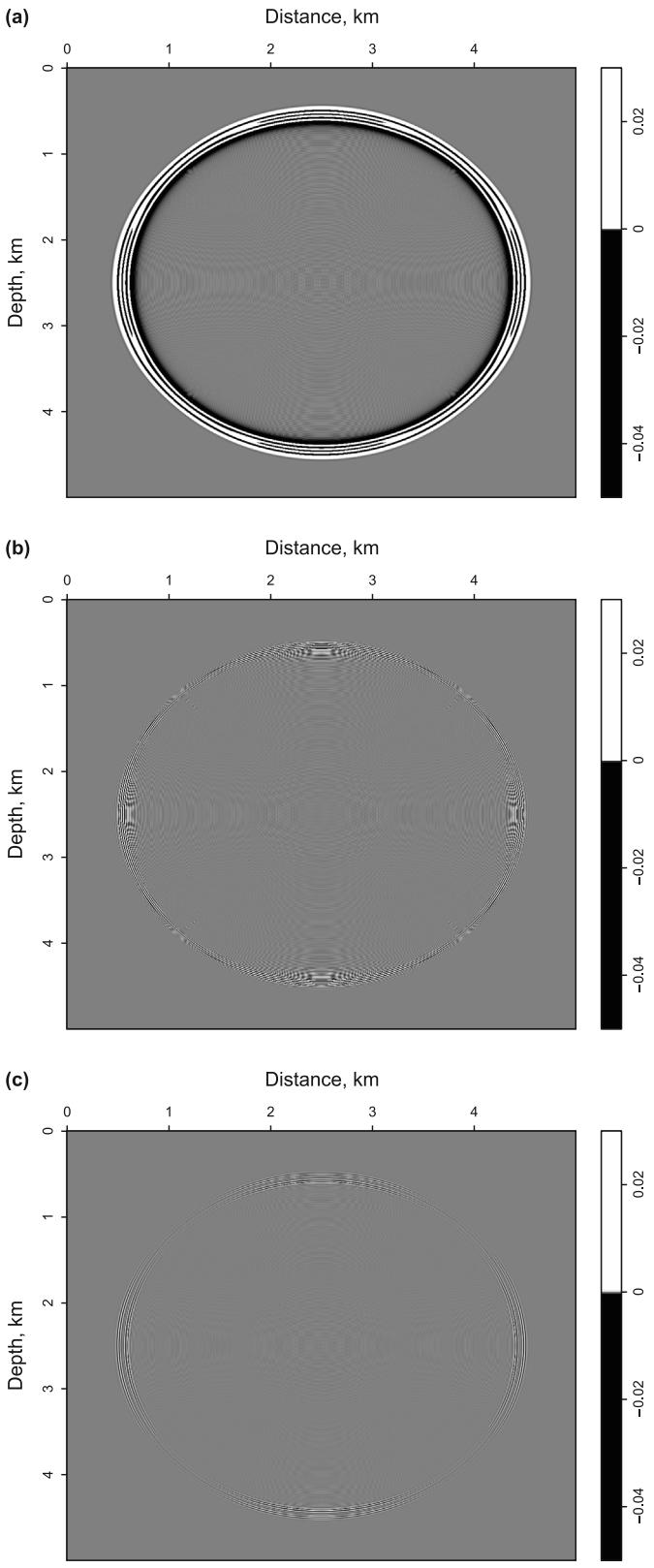

Fig. 7. A comparison of the residual snaps between the snapshots of FD scheme and the snaps of analytical solution. **(a)**, **(b)** and **(c)** are the residual snaps of REA, TES and new method, respectively.

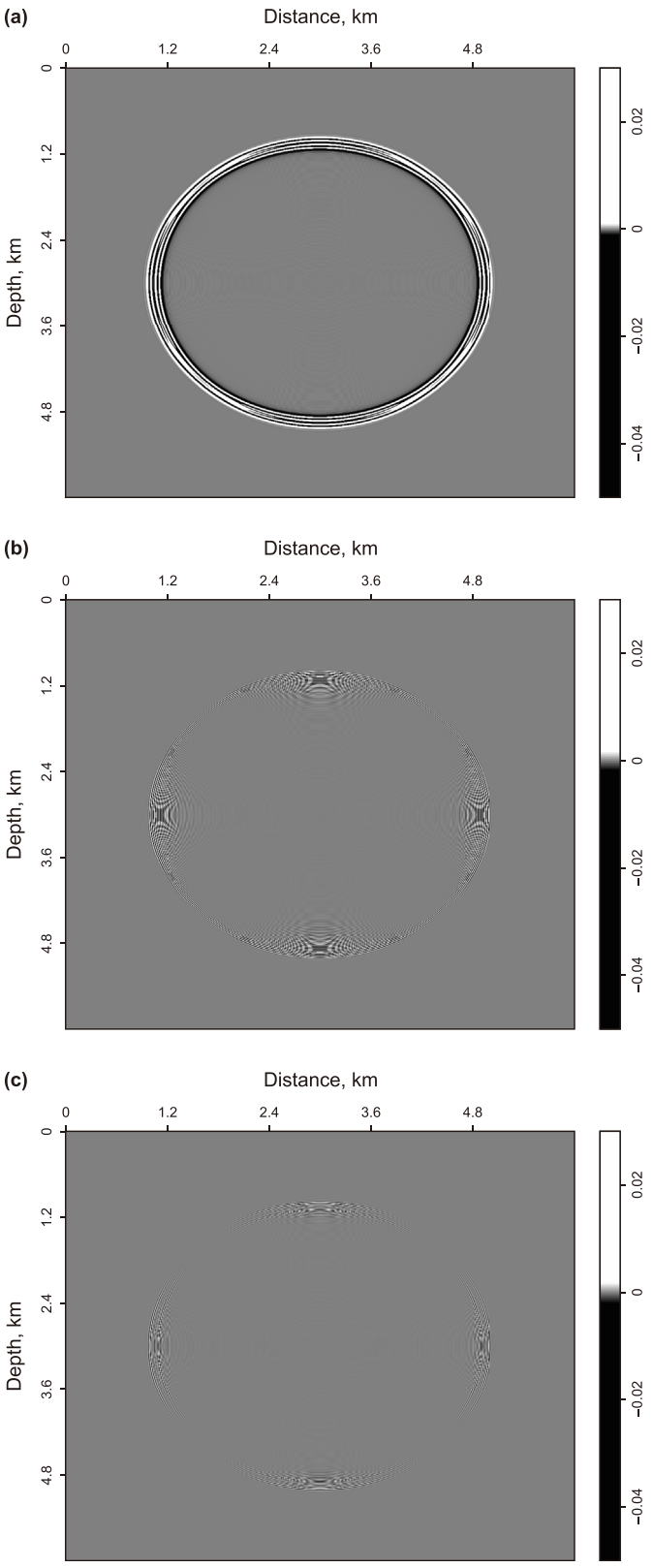

Fig. 8. Comparison of the residual snaps between the snapshots of FD scheme and the snaps of analytical solution when the h changes to 6m. **(a)**, **(b)** and **(c)** are the residual snaps of REA, TES and new method, respectively.

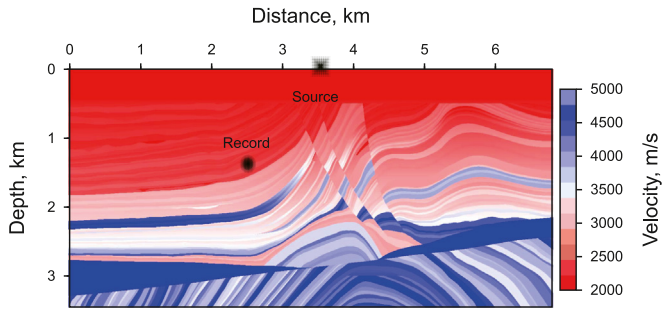

Fig. 9. The inhomogeneous velocity model, highlighting the injected source and record point positions.

geophysical model, we conducted tests using a modified Marmousi model, as shown in Fig. 9. The model was discretized by a 1460×700 grid with a 5 m spatial sampling interval. The source time function was a Ricker wavelet with a dominant frequency of 40 Hz, located at (680 m, 1 m), and a time step of 0.0001 s was used to avoid the accumulation of temporal simulation error. Too large time step leads to instability in the FD scheme (Berland et al., 2007; Tarrass et al., 2011). The propagation was 1.2 s. A pseudo-spectral solution was regarded as the reference solution, because it offered the highest achievable accuracy in this experiment. Fig. 9 shows the recorded point located at (2500 m, 1500 m). All optimization methods were conducted with the same error limitation to simulate wave propagation in inhomogeneous modeling. The optimal FD weights are listed in Table 3.

In this test, the spatial simulation error (E) of the optimized FD weights (REA) is larger than that of TES. In our numerical test, for the optimized method, the residuals of waveform and snapshot are larger than those of the TES, as shown in Figs. 10 and 11. These observations indicate that the optimization algorithm cannot achieve accurate modeling results. Analyzing the residual waveform, as illustrated in Fig. 10, the new method produced the smallest waveform residual in the inhomogeneous model simulation. The new method has a substantial improvement in reducing the residual of the snapshots compared to the TES and REA methods, as shown in Fig. 11. This notable improvement can be attributed to the fact that the new method can minimize the spatial simulation error E.

We then tested the modified Marmousi model injected with a 50 Hz ricker wavelet. The residuals of the snapshot are shown in Fig. 12. With the dominant frequency increase to 50 Hz, the spectrum of the seismic wavelet ($U_w(k)$) changes. According to the calculation in Algorithm 1, the FD weights of the new method computed for these parameters (50 Hz) are the same as those computed for the first set of parameters (40 Hz). In the second inhomogeneous test, the new method showed a substantial improvement in reducing the residual of the snapshots compared with TES and REA, as shown in Fig. 12. In the inhomogeneous model, the new method consistently provides superior performance and robustness in suppressing residuals compared with other computational strategies. When the dominant frequency of the seismic wavelet changes to 50 Hz, the new FD weights computed by the algorithm are identical to those at 40 Hz, as listed in Table 3.

To verify the superiority of the new method in complex media, we conducted a simulation test using vertical transversely isotropy (VTI) media. The velocity model of VTI medium was a new Marmousi model, where the number of grids is 369×188. The velocity

Table 3
The FD weights from different methods in inhomogeneous model simulation.

REA	TES	New method (f_m = 40 Hz)	New method (f_m = 50 Hz)
1.912412497025990	1.777777777784810	1.853644482247890	1.853644482247890
−0.417184277546726	−0.311111111114948	−0.367512353218908	−0.367512353218908
0.146712622154826	0.075420875422329	0.109484475071185	0.109484475071185
−0.058492929938945	−0.017676767677177	−0.034094713508097	−0.034094713508097
0.023249417163344	0.003480963481052	0.009599914818463	0.009599914818463
−0.008430453541392	−0.000518000518014	−0.002184501573063	−0.002184501573063
0.002456117364094	0.000050742907887	0.000347427907264	0.000347427907264
−0.000412354204683	−0.000002428127428	−0.000028432973615	−0.000028432973615

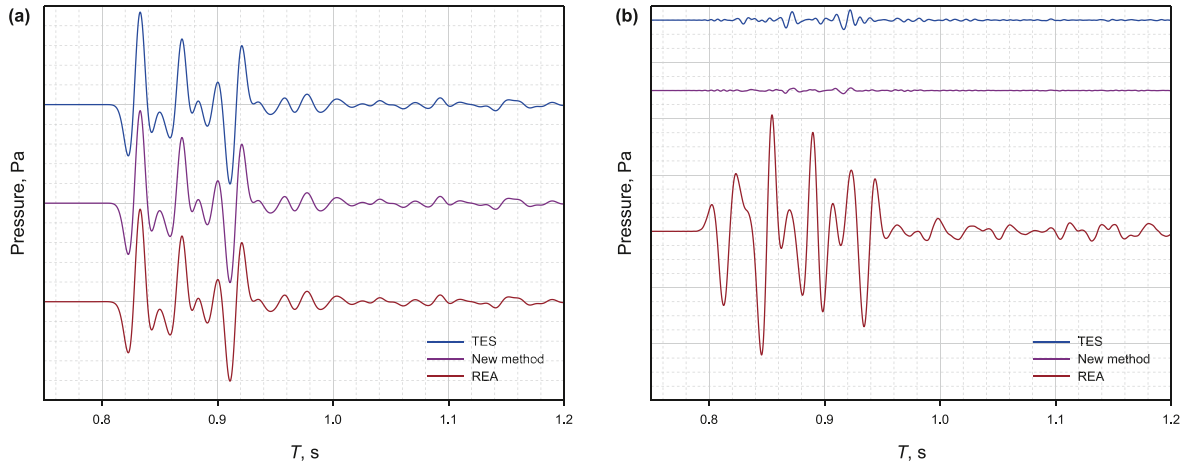

Fig. 10. A comparison of the waveform record located at (2500 m, 1500 m) from all FD weights computational methods. **(a)** Comparison of the original waveform, and **(b)** the comparison of the residual waveform.

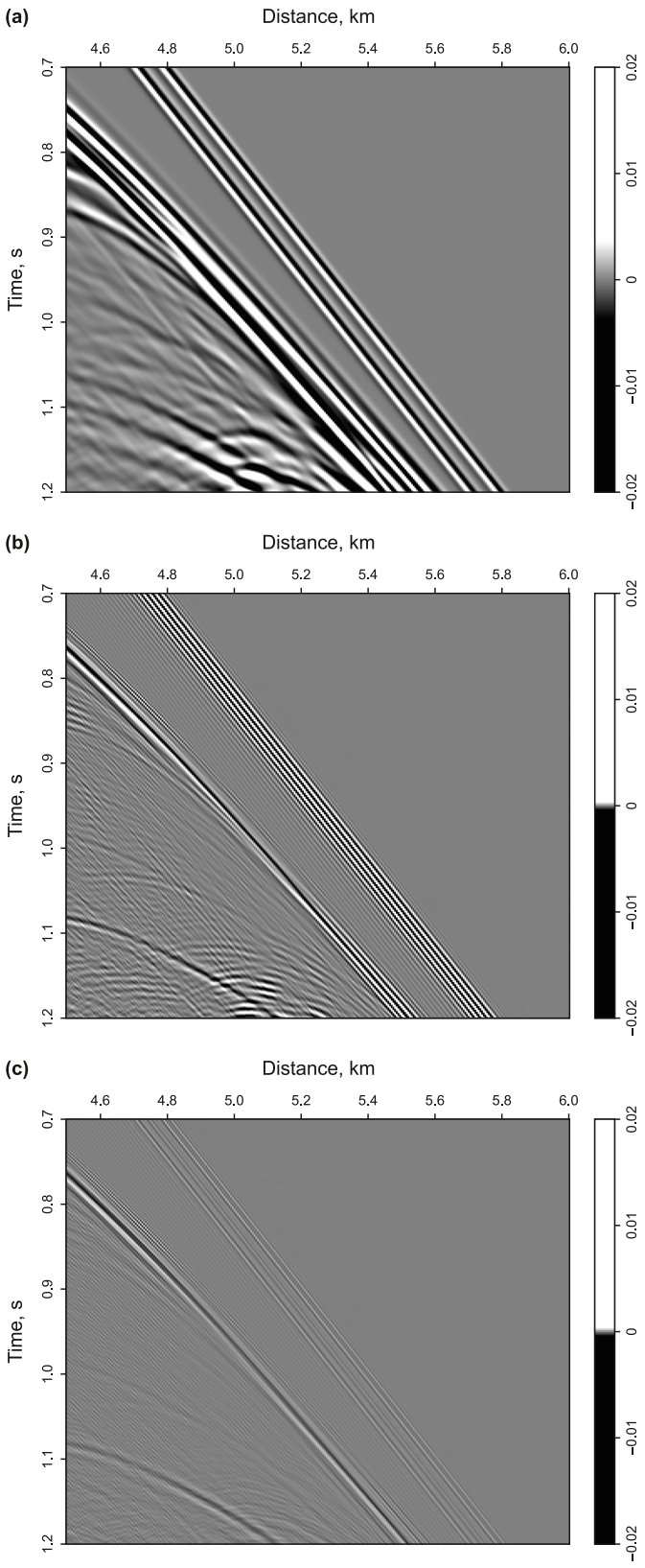

Fig. 11. A comparison of the residual snapshots between the snapshots of FD scheme and the snapshots of the referenced solution. **(a)**, **(b)** and **(c)** are the residual snapshots of REA, TES and new method, respectively. The snapshot of referenced solution is obtained by pseudo-spectral method.

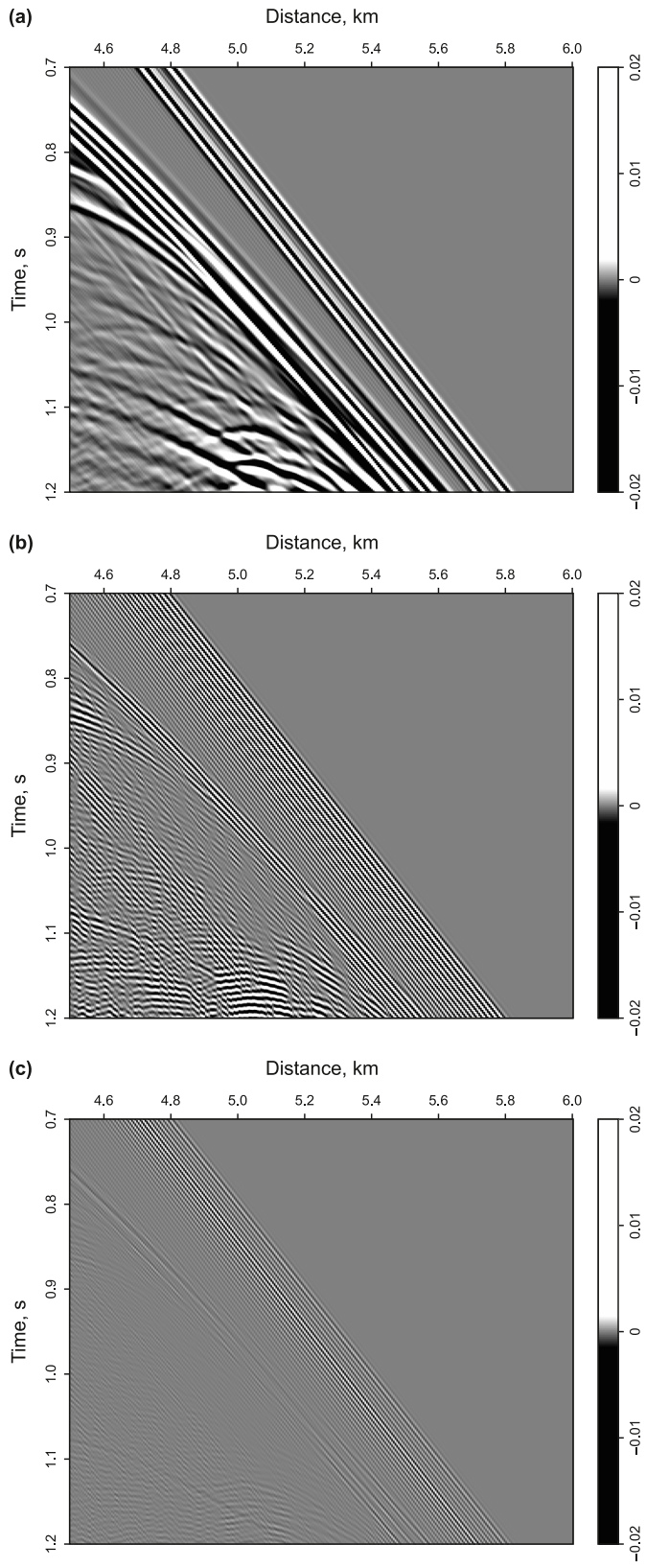

Fig. 12. A comparison of the residual snapshots between the snapshots of FD scheme and the snapshots of the referenced solution when the dominant frequency of wavelet changes to 50 Hz. **(a)**, **(b)** and **(c)** are the residual snapshots of REA, TES and new method, respectively. The snapshot of referenced solution is obtained by pseudo-spectral method.

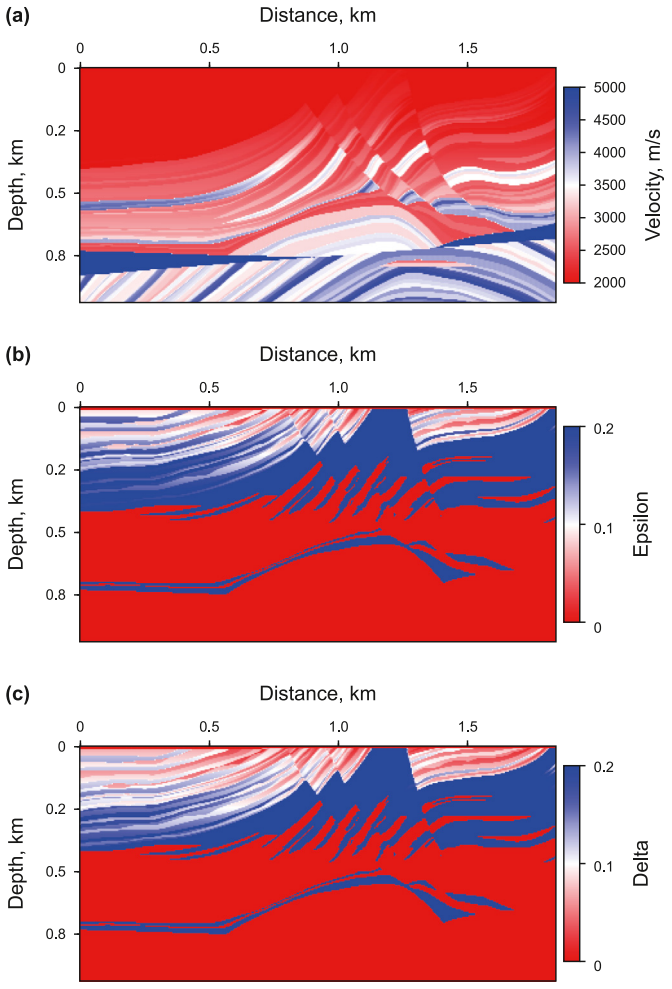

Fig. 13. The velocity model, ε and δ model.

and anisotropic parameter (δ and ε) models were illustrated in Fig. 13, respectively. The spatial sampling interval was 5 m, the time step was 0.0002 s, the propagation time was 0.45 s, and the dominant frequency of the ricker wavelet was 30 Hz. In this test, the FD weights were computed using the REA, TES and proposed method.

Fig. 14 is a combination of residuals of the snapshots for all methods. It can be clearly observed from Fig. 14 that the proposed method exhibited the smallest residual. Notably, some residuals of the snapshot appeared to resemble the model structure, which were the error of pseudo-shear wave during the simulation process, as shown in Fig. 14. It's worth mentioning that the error in the pseudo-shear wave of the optimization method was smaller compared to that of the new method. This is mainly due to the spatial simulation error of the REA method, which is so significant that it masks the error of the pseudo-shear wave. In our test, none of the FD weights was able to effectively mitigate the error of the pseudo-shear wave. How to use the FD weights to reduce the error of the pseudo-shear wave required further research. As evident from the residuals of the snapshots, the new method can significantly enhance the accuracy of forward modeling in VTI media compared with other methods.

5. Discussion

In this paper, our research focused solely on mitigating spatial simulation error, not considered the temporal simulation error. For

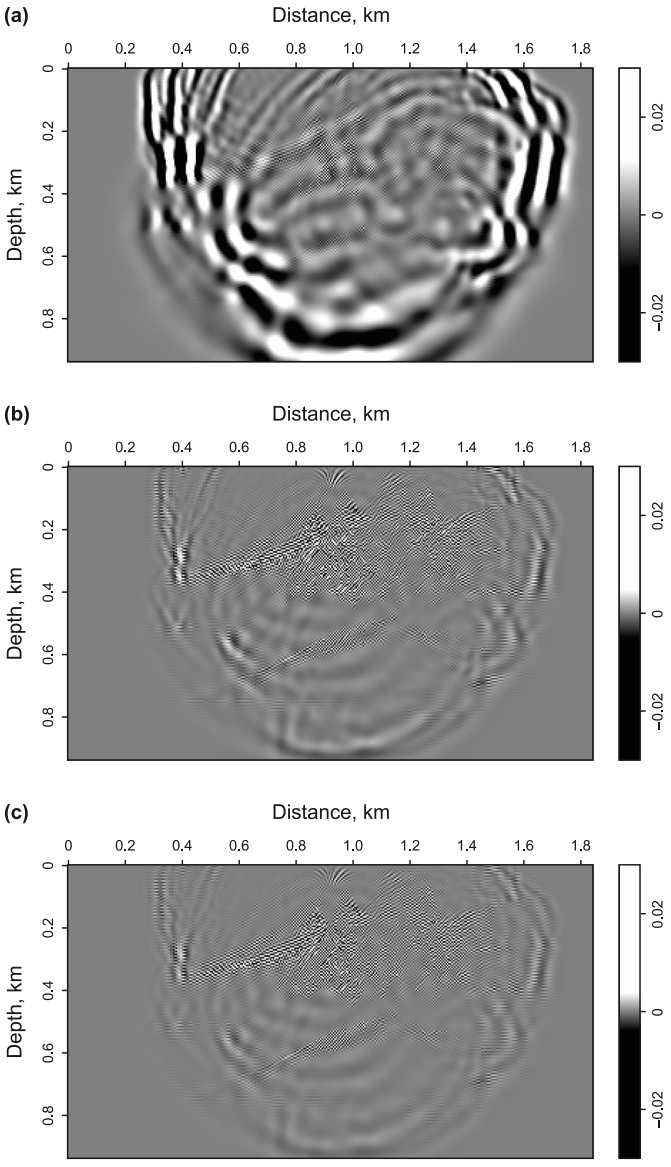

Fig. 14. A comparison of the residual snaps between the snaps of FD scheme and the snaps of referenced solution. **(a)**, **(b)** and **(c)** are the residual snaps of REA, TES and new method, respectively. The snaps of referenced solution are obtained by pseudo-spectral method.

temporal error, previous studies have almost eliminated it. We recommend employing a method known as the inverse time dispersion transform (ITDT) (Koene et al., 2018) to address temporal simulation error. ITDT can eliminate the temporal simulation error, but it requires the computation of the Fourier transform and inverse Fourier transform of the wavefield.

If we wanted to mitigate the temporal simulation error by changing the FD weights, we could construct the cost function based on the phase velocity. The phase velocity considers both the temporal and spatial partial derivatives. Thus, optimizing the phase velocity error can simultaneously mitigate the temporal and spatial simulation errors.

As we derive the phase velocity, we noticed that the spatio-temporal numerical error also has a relation with the spectrum of the seismic wavefield. Therefore, our next objective was to utilize the new method to simultaneously reduce both spatial and temporal numerical errors.

Tam and Webb (1993) proposed the dispersion-relation preserving (PRD) method, which is a similar optimization method based on the L_2 norm function, specifically focusing on optimizing the weights of high-order approximations for temporal derivatives. Etemadsaeed et al. (2016) combined the Taylor expansion (TE) method with PRD to investigate various grid combinations, aiming to develop the most accurate finite-difference (FD) grid scheme. The nature of the two papers is to minimize the deviation between the numerical wavenumber and real wavenumber (for spatial derivation), or minimize the deviation between the numerical frequency and real frequency (for temporal derivation). Our research seeks to minimize the dot product of the difference between numerical wavenumber and real wavenumber with the spectrum of the seismic wavefield.

6. Conclusion

In this paper, we derived the specific process for calculating spatial simulation error and found this error is determined by the dot product of the spectrum of the seismic wavefield with the spatial dispersion relation. However, in previous research, the FD weights optimization method was only focused on minimizing the error of dispersion relation. Consequently, in some scenarios, optimized FD weights could lead to an increase in the simulation error. Therefore, based on the objective of minimizing simulation error, we designed an optimization problem to output FD weights. Subsequent simulation experiments in the homogeneous and inhomogeneous model tests demonstrated the effectiveness of the new method in suppressing spatial simulation errors in various scenarios.

CRediT authorship contribution statement

Wei-Ting Peng: Writing – review & editing, Writing – original draft, Visualization, Validation, Supervision, Software, Resources, Project administration, Methodology, Investigation, Funding acquisition, Formal analysis, Data curation, Conceptualization. **Jian-Ping Huang:** Conceptualization.

Declaration of competing interest

The authors declare that they have no known competing financial interests or personal relationships that could have appeared to influence the work reported in this paper.

Acknowledgement

This study is supported by the Marine S&T Fund of Shandong Province for Pilot National Laboratory for Marine Science and Technology (No. 2021QNLM020001), the Major Scientific and Technological Projects of Shandong Energy Group (No. SNKJ2022A06-R23), the Funds of Creative Research Groups of China (No. 41821002), the Major Scientific and Technological Projects of CNPC (No. ZD2019-183-003).

Appendix

The stability analysis

For a finite-difference scheme, the stability problem is important, thus, we discussed the stability of new method in this section. We could draw the stability of FD scheme by using the equation (Liu, 2020) as follow:

$$\frac{v_{\max}\tau}{h} \le \left(2\sum_{m=1}^{\mathrm{int}((M+1)/2)} c_{2m-1}\right)^{-\frac{1}{2}} \tag{A.1}$$

where the $v_{\max}$ was the maximal velocity of the model, the τ was the time step. If the model parameters satisfy Eq. (A.1), the numerical modeling can perform stably.

The maximum Courant-Friedrichs-Lewy (CFL) number $C_{\max}$ can be written as

$$C_{\max} = \left(2\sum_{m=1}^{\mathrm{int}((M+1)/2)} c_{2m-1}\right)^{-\frac{1}{2}} \tag{A.2}$$

which is the same as that presented at Liu (2020). Based on Eq. (A.1) and (A.2), when the $\frac{v_{\max}\tau}{h} < C_{\max}$, the simulation was stable. So, we can used the $C_{\max}$ to compare the stability of FD weights. As Fig. A.1 shows, both the optimization method and the new method had a lower stability than the TES. This phenomenon was attributed to the negative relation between stability and bandwidth, as shown in Liu (2020). The FD weights from the new method used for stability testing and those used for the numerical simulations in the homogeneous acoustic medium are the same set of FD weights.

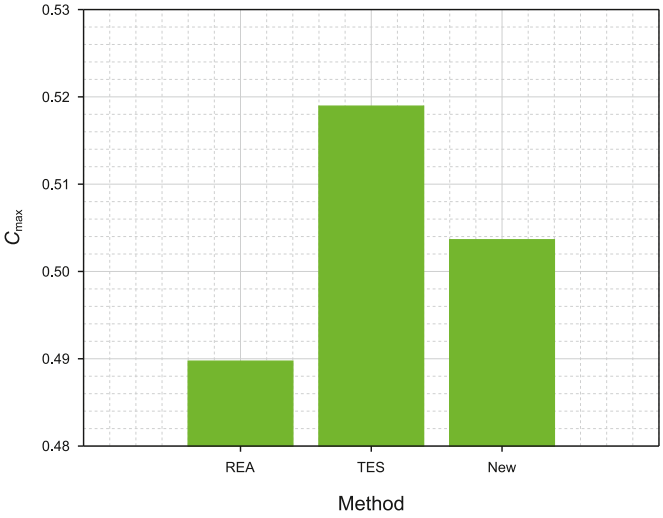

Fig. A.1. A comparison of the stability for different FD weights. The $C_{\max}$ is computed based on Eq. (A.2).

References

Alford, R.M., Kelly, K.R., Boore, D.M., 1974. Accuracy of finite-difference modeling of the acoustic wave equation. Geophysics 39 (6), 834–842. https://doi.org/10.1190/1.1440470.

Alterman, Z., Karal, F.C.J., 1968. Propagation of elastic waves in layered media by finite difference methods. Bull. Seismol. Soc. Am. 58 (1), 367–398. https://doi.org/10.1785/BSSA0580010367.

Berland, J., Bogey, C., Marsden, O., Bailly, C., 2007. High-order, low dispersive and low dissipative explicit schemes for multiple-scale and boundary problems. J. Comput. Phys. 224 (2), 637–662. https://doi.org/10.1016/j.jcp.2006.10.017.

Chu, C.L., Stoffa, P.L., 2012. Determination of finite-difference weights using scaled binomial windows. Geophysics 77 (3), W17–W26. https://doi.org/10.1190/geo2011-0336.1.

Chu, C.L., Stoffa, P.L., Seif, R., 2009. High-order Rotated Staggered Finite Difference Modeling of 3D Elastic Wave Propagation in General Anisotropic Media. SEG Technical Program Expanded Abstracts 2009, 291–295. https://doi.org/10.1190/1.3255458.

Dablain, M.A., 1986. The application of high-order differencing to the scalar wave equation. Geophysics 51 (1), 54–66. https://doi.org/10.1190/1.1442040.

Etemadsaeed, L., Moczo, P., Kristek, J., Ansari, A., Kristekova, M., 2016. A no-cost improved velocity-stress staggered-grid finite-difference scheme for modelling seismic wave propagation. Geophys. J. Int. 207, 481–511. https://doi.org/10.1093/gji/ggw287.

Etgen, J.T., 2007. A tutorial on optimizing time domain finite-difference schemes:

"Beyond Holberg". Stanford Exploration Project 129, 33–43.
Fornberg, B., 1995. Calculation of weights in finite difference formulas. Society for Industrial and Applied Mathematics 40 (3), 685–691.
He, Z., Zhang, J.H., Yao, Z.X., 2019. Determining the optimal weights of the explicit finite-difference scheme using the Remez exchange algorithm. Geophysics 84 (3), S137–S147. https://doi.org/10.1190/geo2018-0446.1.
Holberg, O., 1987. Computational aspects of the choice of operator and sampling interval for numerical differentiation in large-scale simulation of wave phenomena. Geophys. Prospect. 35 (6), 629–655. https://doi.org/10.1111/j.1365-2478.1987.tb00841.x.
Igel, H., Mora, P., Riollet, B., 1995. Anisotropic wave propagation through finite-difference grids. Geophysics 60 (4), 1203–1216. https://doi.org/10.1190/1.1443849.
Kelly, K., Ward, R., Treitel, S., Alford, R.M., 1976. Synthetic seismograms a finite-difference approach. Geophysics 41 (1), 2–27. https://doi.org/10.1190/1.1440605.
Kindelan, M., Kamel, A., Sguazzero, P., 1990. On the construction and efficiency of staggered numerical differentiators for the wave equation. Geophysics 55 (1), 107–110. https://doi.org/10.1190/1.1442763.
Koene, E.F.M., Robertsson, J.O.A., 2020. Optimal finite-difference operators for arbitrarily sampled data. Geophysics 85 (1), F39–F51. https://doi.org/10.1190/geo2019-0081.1.
Koene, E.F.M., Robertsson, J.O.A., Broggini, F., Andersson, F., 2018. Eliminating time dispersion from seismic wave modeling. Geophys. J. Int. 213, 169–180. https://doi.org/10.1093/gji/ggx563.
Levander, A.R., 1988. 4th-order finite-difference P-SV seismograms. Geophysics 53 (11), 1425–1436. https://doi.org/10.1190/1.1442422.
Liu, Y., 2013. Globally optimal finite-difference schemes based on least squares. Geophysics 78 (4), T113–T132. https://doi.org/10.1190/geo2012-0480.1.
Liu, Y., 2014. Optimal staggered-grid finite-difference schemes based on least-squares for wave equation modelling. Geophys. J. Int. 197 (2), 1033–1047. https://doi.org/10.1093/gji/ggu032.
Liu, Y., 2020a. Maximizing the CFL number of stable time-space domain explicit finite-difference modeling. J. Comput. Phys. 416 (1), 1–17. https://doi.org/10.1016/j.jcp.2020.109501.
Liu, Y., 2020b. Acoustic and elastic finite-difference modeling by optimal variable-length spatial operators. Geophysics 85 (2), T57–T70. https://doi.org/10.1190/geo2019-0145.1.
McClellan, J., Parks, T., Rabiner, L., 1973. A computer program for designing optimum FIR linear phase digital filters. IEEE Trans. Audio Electroacoust. 21 (6), 506–526. https://doi.org/10.1109/TAU.1973.1162525.
Miao, Z.Z., Zhang, J.H., 2020. Reducing error accumulation of optimized finite-difference scheme using minimum norm. Geophysics 85 (5), T275–T291. https://doi.org/10.1190/geo2019-0758.1.
Peng, W.T., Huang, J.P., Shen, Y., 2023. Reducing the low-wavenumber dispersion error by building the Lagrange dual problem with a powerful local restriction. J. Geophys. Eng. 20 (4), 798–815. https://doi.org/10.1093/jge/gxad047.
Remez, E.Y., 1934. Sur la détermination des polynômes d'approximation de degré donnée. Communications of the Kharkov Mathematical Society 10, 41–63.
Ren, Z.M., Liu, Y., 2015. Acoustic and elastic modeling by optimal time-space-domain staggered-grid finite-difference schemes. Geophysics 80 (1), T17–T40. https://doi.org/10.1190/geo2014-0269.1.
Shao, Z.H., Wei, G.W., Zhao, S., 2003. DSC time-domain solution of Maxwell's equations. J. Comput. Phys. 189 (2), 427–453. https://doi.org/10.1016/S0021-9991(03)00226-2.
Tam, C.K.W., Webb, J.C., 1993. Dispersion-relation-preserving finite difference schemes for computational acoustics. J. Comput. Phys. 107, 262–281. https://doi.org/10.1006/jcph.1993.1142.
Tarrass, I., Giraud, L., Thore, P., 2011. New curvilinear scheme for elastic wave propagation in presence of curved topography. Geophys. Prospect. 59 (5), 889–906. https://doi.org/10.1111/j.1365-2478.2011.00972.x.
Wang, Y., Wu, R.S., 2002. An optimal spatial finite-difference operator which reduces truncation error to a minimum. Adv. Atmos. Sci. 19 (3), 468–486. https://doi.org/10.1007/s00376-002-0080-2.
Wang, Y.F., Liang, W.Q., Nashed, Z., Li, X., Liang, G.H., Yang, C.C., 2014. Seismic modeling by optimizing regularized staggered-grid finite-difference operators using a time-space-domain dispersion-relationship-preserving method. Geophysics 79 (5), T277–T285. https://doi.org/10.1190/geo2014-0078.1.
Xiao, F., Tang, X.H., Zhang, X.J., 2006. Comparison of Taylor finite difference and window finite difference and their application in FDTD. J. Comput. Appl. Math. 193 (2), 516–534. https://doi.org/10.1016/j.cam.2005.05.030.
Yang, L., Yan, H.Y., Liu, H., 2017a. An optimal implicit staggered-grid finite-difference scheme based on the modified Taylor-series expansion with minimax approximation method for elastic modeling. J. Appl. Geophys. 138, 161–171. https://doi.org/10.1016/j.jappgeo.2017.01.020.
Yang, L., Yan, H.Y., Liu, H., 2017b. Optimal staggered-grid finite-difference schemes based on the minimax approximation method with the Remez algorithm. Geophysics 82 (1), T27–T42. https://doi.org/10.1190/geo2016-0171.1.
Yong, P., Huang, J.P., Li, Z.C., Liao, W.Y., Qu, L.P., Li, Q.Y., Liu, P.J., 2017. Optimized equivalent staggered-grid FD method for elastic wave modelling based on plane wave solutions. Geophys. J. Int. 208 (2), 1157–1172. https://doi.org/10.1093/gji/ggw447.
Zhang, J.H., Yao, Z.X., 2013a. Optimized explicit finite-difference schemes for spatial derivatives using maximum norm. J. Comput. Phys. 250 (1), 511–526. https://doi.org/10.1016/j.jcp.2013.04.029.
Zhang, J.H., Yao, Z.X., 2013b. Optimized finite-difference operator for broadband seismic wave modeling. Geophysics 78 (1), A13–A18. https://doi.org/10.1190/geo2012-0277.1.
Zhou, B., Greenhalgh, S.A., 1992. Seismic scalar wave equation modeling by a convolutional differentiator. Bull. Seismol. Soc. Am. 82 (1), 289–303. https://doi.org/10.1785/BSSA0820010289.